https://doi.org/10.1016/j.conbuildmat.2024.135042

Roles of ultra-fine waste glass powder in early hydration of Portland cement: Hydration kinetics, mechanical performance, and microstructure

Wing Lun Lam, Yamei Cai, Keke Sun, Peiliang Shen[+], Chi Sun Poon[*]

Department of Civil and Environmental Engineering, The Hong Kong Polytechnic University, Hung Hom, Kowloon, Hong Kong

Corresponding author. Email address:+ peiliang.shen@polyu.edu.hk (P. Shen), cecspoon@polyu.edu.hk (C.S.Poon)

Abstract

Reutilising waste glass powder (WGP) could be a promising alternative to supplementary cementitious materials (SCMs) because of its availability and carbon footprint reduction, especially in Hong Kong. However, concerns about the adverse effects on hydration and early strength have been raised and might limit concrete application. A wet grinding method was applied to convert WGP into ultra-fine particles, which could address these concerns and promote the application of WG as an alternative local SCM with a low carbon footprint. This study investigated the effect of wet grinding on WGP's physicochemical properties and how wet-ground WGP modified early hydration kinetics, mechanical performance, and microstructure of cement paste. The results indicated that ultra-fine WG was produced with the D_{50} of 500 nm and modified surface composition. Unlike micro-sized WGP, introducing ultra-fine WGP increased the 1-d strength by 50 % and the 28-d strength by 5 % of cement paste. The improvement of early strength could be attributed to three reasons. Firstly, the dissolution of ultra-fine WGP increased pH in the pore solution of the cement paste, which accelerated the hydration of C_3A and C_3S and promoted the precipitation of ettringite and the formation of C-S-H. Secondly, the submicron particles provided nucleation sites for C-S-H precipitation and increased the pozzolanic reactivity. Lastly, ultra-fine WGP could also effectively fill the pores in the cement paste, leading to a denser microstructure. According to the result, the reactivity of WG could be enhanced

through wet-grinding and finely ground WGP could substitute reactive but costly binders, such as cement and silica fume.

Keywords: Waste glass powder; Cement; Hydration; Microstructure; Pozzolanic reaction

1. Introduction

Rapid population growth has resulted in expanded urbanisation and construction to satisfy the demand for living [1], leading to a rapid increase in the global consumption of construction materials. Concrete production reached 14.0 billion m^3 in 2020 [2]. Concrete production consumes a considerable amount of energy and releases a massive amount of CO_2 [3], contributing to 8.6 % of global anthropogenic CO_2 emissions [4-6] and being one of the major causes of global warming and climate change [7]. Meanwhile, low carbon emissions or "Carbon neutrality" has become a worldwide trend for stabilising the rise in temperature within 1.5 – 2 °C, as agreed on in the Paris Climate Change Conference [8-10]. Thus, reducing CO_2 emissions from the cement sector would greatly aid in the battle against rising temperatures and climate change.

Cement contributes to the primary CO_2 emissions of concrete [5], and thus, reducing the cement dosage in concrete would be the most viable way to mitigate CO_2 emissions, such as utilising SCMs to partially replace cement [11]. However, when selecting suitable SCMs, the availability that satisfies local demands should be considered. For instance, in Hong Kong, only 0.2 million tons of local pulverised fly ash (PFA) are produced annually [12], while the demand is approximately double the local supply [13]. The supply of PFA, a by-product of burning coal, is expected to be more limited because of the future closing down of coal-burning power stations to achieve carbon neutrality [14]. Therefore, exploring alternative SCMs with sufficient local supplies is essential for implementing the strategy to reduce CO_2 emissions in the concrete sector.

WGP is a promising alternative SCM because of improved concrete performance and availability in some areas, especially in Hong Kong. The daily production of glass bottles in Hong Kong was approximately 300 tonnes, while less than 20 % of the consumed glass bottles were recycled in 2020, and the rest were disposed of at landfills [15]. A similar scenario was also observed in the United States. According to the Environmental Protection Agency in the United States, the recycling rate of glass bottles was 31.3 % in 2018, but more than 60 % of glass bottles were disposed of at landfills [16]. Moreover, the application of recycled WG is limited. In Hong Kong, the WG cullet mainly replaces fine aggregates in producing concrete paving blocks [17]. Many studies have proven the better workability, enhanced strength development, and durability of cementitious materials incorporating WGP [18-20]. The improved performance is attributed to the pozzolan reaction and filler effect of WGP, leading to dense microstructure [21]. Therefore, WG has excellent potential to be a widely used SCMs in these areas.

However, some concerns have been raised when using WG in an application. The main factor hindering the utilisation of WG is the potential alkali-silica reaction (ASR) [22, 23] between $Si(OH)_4$ and alkalis, including Na^+, K^+ and Ca^{2+}, forming ASR gel [24]. The ASR gel could produce internal expansive stress when absorbing moisture and damage the concrete structure. Apart from the concern of ASR, the relatively lower pozzolanic reactivity and retarding effect of WGP compared to GGBS and FA also hinder WGP's ability to replace GBS and FA. Incorporating WGP in concrete could result in delayed hydration, lengthened setting time and reduced early strength, particularly when a high proportion of WGP (more than 20 %) was incorporated [22, 25, 26]. Approaches such as thermal treatment and adding reactive nanoparticles have been introduced to improve the early strength of WGP concrete [27-29]. However, these methods could significantly increase production costs and energy consumption.

74 The particle size of WG is the most critical factor that significantly controls the ASR and
75 pozzolanic reactivity [30, 31]. Thus, grinding WGP into finer particles could be a viable
76 approach to mitigate ASR and enhance the pozzolanic reactivity. Previous studies
77 demonstrated that finer particle size can effectively reduce ASR expansion [28, 32]. The
78 observation was attributed to preventing concentrated expansive silica [33]. Moreover, finer
79 WGP would be expected to have higher reactivity because of the higher surface area [34, 35].
80 However, conventional dry grinding treatment could only produce WGP in the micron size
81 range, which had been found to have a lower reactivity [30]. Compared with other reactive
82 SCMs such as SF, WGP was less reactive due to the large particle size [29] and grinding the
83 WGP as fine as SF might increase the reactivity and substitute SF.
84 Wet grinding might be an alternative to produce finer WGP and enhance its reactivity. The
85 mechanism of wet grinding to refine the powdered raw materials into submicron size is through
86 the impaction, shear stress and friction between the grinding balls and the raw materials in a
87 liquid environment [36]. The ions on the surface of the powdered particles could be dissolved
88 into the liquid media, resulting in a modified surface structure of the raw material and increased
89 reactivity [36]. Another benefit of wet grinding compared with dry grinding was an energy
90 saving of approximately 50 % to produce a material with the same particle size [37]. For
91 instance, previous studies on slag [36, 38, 39] and fly ash [40-42] demonstrated that wet
92 grinding efficiently increased early and later strength. Therefore, wet grinding could also be
93 used in the mechanical activation of WG. A recent study indicated that activated WGP via 120
94 mins of wet-grinding demonstrated accelerated cement hydration [43]. Another study
95 demonstrated that wet-grinded WGP could enhance the 1-d compressive strength of mortar and
96 refine the pore structure [44]. These studies provided evidence of improved performance by
97 incorporating wet-grinded WG. However, these studies did not explain how the wet grinding

modified the physicochemical properties of WG, which contributed to the modification in early hydration kinetics, mechanical performance, and microstructure of cement pastes.

Therefore, the motivation of this paper was to introduce a wet-grinding treatment to enhance the reactivity of WGP to replace some costly cementitious materials, such as cement and SF. This study aims to discover the effect of wet grinding on the physicochemical properties of WGP and how the early hydration kinetics, mechanical performance and microstructure of cement paste were modified. This study attempted to activate WGP by wet-grinding and investigated the chemical composition, surface composition, particle size distribution and morphologies of ultra-fine WGP. Moreover, the mechanisms of how ultra-fine WGP affect early cement hydration, mechanical performance and microstructure were systematically studied based on the analysis of hydration kinetics, hydrate production, microstructure, and pore solution.

2. Materials and methods

2.1 Materials and characterisation

An ASTM type I class 52.5 Ordinary Portland Cement (OPC) was used in this study. The WGP was produced from a waste glass cullet (WGC) sourced from a waste recycling facility in Hong Kong. WGC was ground in a ball mill for 90 mins to WGP with a D_{50} of approximately 20 μm before wet-grinding treatment (described in Section 2.2). The particle size distribution of cement (Fig. *1*) was obtained by a laser diffraction particle size 144 analyser (Malvern Mastersizer 3000E). The mineral compositions of OPC and ultra-fine WGP were characterised by Rietveld refinement of quantitative X-ray diffraction (Q-XRD) shown in Table 1. The chemical compositions of OPC and 20 μm and 500 nm WGP shown in Table 2 were determined by X-ray fluorescence (Rigaku Supermini 200 spectrometer). The result shows that the content of Na_2O in WGP was reduced after wet-grinding treatment. The reduction of Na_2O content

could be attributed to the dissolution of Na^+ from WGP during wet-grinding treatment while the supernatant was removed. Only the solids were used for the experiment.

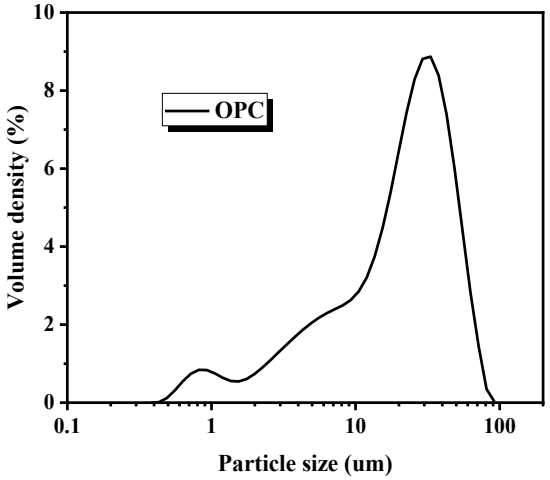

Fig. 1 Particle size distribution of OPC

Table 1 Mineral composition of cementitious materials (%)

	C_3S	C_2S	C_3A	C_4AF	Gypsum	Calcite
OPC	61.82	13.05	8.40	8.70	2.08	5.95
WGP (500 nm)	Amorphous					

Table 2 Chemical compositions of cementitious materials (%)

Compositions	SiO_2	CaO	Fe_2O_3	MgO	SO_3	Al_2O_3	K_2O	Na_2O	P_2O_5
OPC	19.1	65.2	2.96	0.75	4.27	6.06	0.68	0	0.14
WGP (20 μm)	69.2	10.6	0.63	1.43	0.17	2.27	0.78	14.5	0.12
WGP (500 nm)	71.1	12.6	1.17	1.73	0.07	2.45	0.85	9.76	0.12

2.2 The preparation process of ultra-fine WGP

A mixture of 20 g of the 20 μm WGP produced by conventional dry grinding, 120 g of tap water and 3 g of polycarboxylate ether (PCE) superplasticiser (Sika) with a specific gravity of 1.05 were wet ground in a planetary ball mill with agate tanks and balls in Fig. 2 (mass ratio of

20 mm: 10 mm: 6 mm = 3:50:90) for 30 mins at a speed of 450 rpm. The superplasticiser was used to facilitate the dispersion of WGP during wet grinding treatment. The solids of the post-grinding mixture were collected using a centrifuge operating at 10,000 rpm for 10 min (Dynamica, Velocity 18R) and dried at 105°C overnight in an oven.

(a) Agate Tank (1 L)

(b) Agate balls

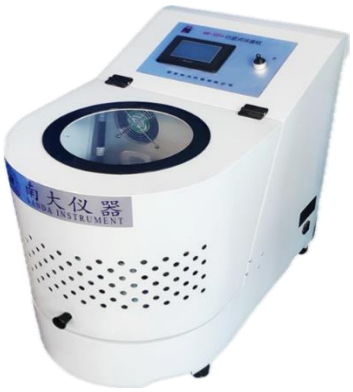

(c) Planetary ball mill

Fig. 2 Equipment for wet grinding

2.3 Design mix of ultra-fine WGP paste and specimen preparation

The WGP cement paste was prepared based on the mix proportions in Table *3*. The water-to-binder ratio (w/b) for all the specimens was 0.4. Due to the flocculation of ultra-fine WGP, ultra-fine WGP was mixed with water and dispersed by ultrasound for 30 mins. Afterwards, the paste specimens were prepared by mixing cement and the ultra-fine WGP slurry in a mixer at low speed for 1 min, followed by at high speed for 3 mins. Then, the paste was remixed at a low speed for 1 min to remove the bubbles produced from the high-speed mixing.

Table 3 Design mix of ultra-fine WGP paste

Mix	Cement	WGP	w/(cement+WGP)
Ref	1	0	
1%	0.99	0.01	
3%	0.97	0.03	0.4
5%	0.95	0.05	
7%	0.93	0.07	

2.3 Physicochemical properties test of ultra-fine WG

The physicochemical properties of ultra-fine WGP were characterised using several amounts of equipment. A Malvern Zetasizer Nano Series was used to determine the ultra-fine WGP. In addition, the zeta potential of ultra-fine WGP was also acquired using a Nano-Series Zetasizer. WGP and deionised water were mixed in a mass ratio of 1:10000, and 1 mL of the mixture was injected into a folder capillary cell to determine the zeta potentials. The surface composition of the ultra-fine WGP sample was characterised by Nexsa X-ray photoelectron spectroscopy (XPS, Thermo Scientific, America). The analytical software CASAXPS was used to analyse the XPS spectrum of ultra-fine WGP. Scanning electron microscopy (SEM, TESCAN VEGA3) was conducted to observe the morphology of the ultra-fine WGP.

2.4 Fresh properties

The slump flow of WGP cement pastes was measured according to BS EN1015-3 [45]. The test was performed immediately after mixing. In addition, a Vicat apparatus was used to determine the samples' initial and final setting times according to the BS EN 196-3 procedures [46].

2.5 Mechanical properties

(1) macro-mechanical properties

The WGP cement pastes were cast in steel cube moulds of 20 mm × 20 mm × 20 mm to determine the 1-d, 7-d and 28-d compressive strength. The specimens were vibrated on a

166 vibration table and sealed with plastic wrap to prevent surface moisture loss. The specimens
167 were demolded at 24h and cured in a CaO-saturated solution until the testing time. A 2 mm/min
168 loading rate was applied for the compressive strength test.
169 (2) micro-mechanical properties
170 Nano-indentation was conducted to investigate the early micro-/nano-mechanical properties of
171 the cement paste using a nano-indenter (Bruker's Hysitron TI Premier). The instrument was
172 equipped with a Berkovich diamond tip with a triangular pyramid shape. The 72-h paste
173 specimens used for nano-indentation were fractured and impregnated in epoxy resin. The
174 surface of the impregnated paste was polished according to the procedures reported in previous
175 literature [47]. Before the measurement, the nano-indenter was first calibrated on a standard
176 sample of fused quartz. The measurement was conducted according to the setup of the
177 indentation program illustrated in Fig. 3. A 15 × 15 square grid arrangement (225 points total)
178 with a 10 μm spacing was used to investigate the micro-/nano-mechanical properties. The
179 loading for indentation was a trapezoid load with a loading rate of 400 μN/s to reach 2000 μN,
180 a holding time of 2 s and an unloading speed of 400 μN/s. The result after measurement
181 provided the reduced modulus (E_r) and hardness (H) of the cement paste. The reduced modulus
182 was a combined modulus of the specimen and indenter and can be converted to the indentation
183 modulus based on Equation (1) [48]:

$$E' = \left(\frac{1}{E_r} - \frac{1-v_i^2}{E_i}\right)^{-1} \quad (1)$$

184 Where E' is the indentation modulus. E_i and v_i are the modulus and Poisson's ratio of the
185 indenter, respectively. For a diamond tip, E_i = 1140 GPa and $v_i = 0.07$ were used in this study
186 [49].

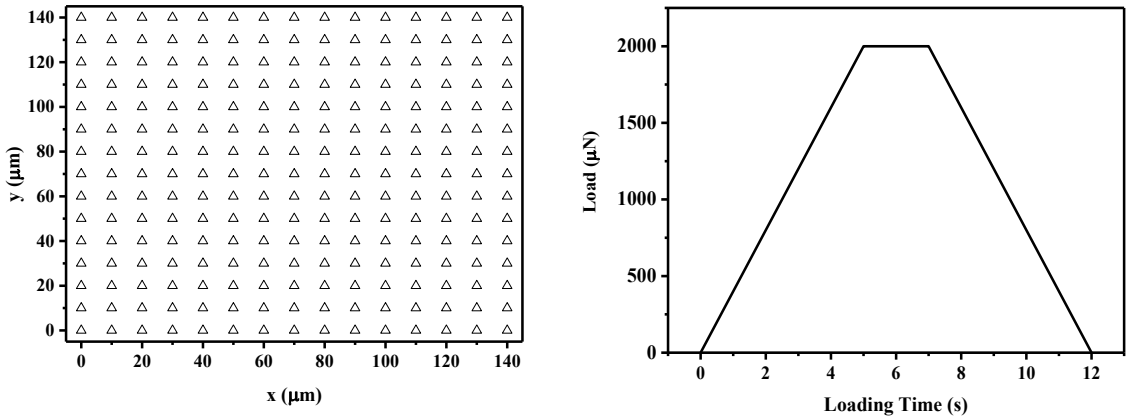

(a) (b)

Fig. 3 (a) Grid setting for nano-indentation; (b) Loading program of nano-indentation test

2.6 Hydration heat

The heat flow and cumulative heat of the pastes were determined by TAM (TA instruments Microcalorimetry) Air isothermal calorimeter for 72 h. Approximately 20 g of paste samples were premixed with water externally and placed in a glass ampoule sealed with an aluminium cap before being loaded into the calorimeter. A reference ampoule containing dry sand and distilled water with the equivalent total heat capacity was also loaded into the calorimeter to minimise experiment errors. The final heat flow curves were adjusted by the baseline measured before and after the tests.

2.6 Pore solution

The pore solution chemistry of the paste specimens was studied to investigate the mechanism of ultra-fine WGP on cement hydration. 3 % cement replacement by ultra-fine WGP was chosen to compare with the reference. The paste samples were prepared and cast into 50 mL lab tubes sealed with a cap. The hydration was stopped by immersing in liquid nitrogen and being freeze-dried in a freeze-dryer for 1 h. To prepare the pore solution, Ex situ leaching was performed to analyse the pH value and ion concentration [50]. After drying, the paste samples were ground into less than 75 μm. The ground samples were then mixed with DI water in a

mass ratio of 1:1 for 5 mins. The leaching solutions were separated from the ground samples using a centrifuge and were filtrated through a 0.45 μm membrane filter before analysis. The pH of the solution was measured immediately using a portable pH meter. After pH measurement, the solution was stored in a fridge at 5 °C ± 1 °C. The pH was converted to the concentration of OH^- using Equations (2) and (3):

$$pH = 14 - pOH \quad (2)$$

$$pOH = -\log [OH^-] \quad (3)$$

The evolution of pore solution chemistry in the early hydration (up to 72 h) of cement incorporating ultra-fine WGP was studied. Al, Ca, Na, and K concentrations in the pore solution were analysed by an inductively coupled plasma/optical emission spectroscopy (ICP-OES, FMX36, SPECTROBLUE). The pore solutions were digested with concentrated nitric acid and diluted with 5 % nitric acid before the ICP-OES analysis. A geochemical modelling program PHREEQC with a thermodynamic database for cement paste was used to analyse the evolution of the saturation index (SI) of the above ions [51].

2.7 Microstructure

SEM (TESCAN VEGA 3) was used to study the morphology of the ultra-fine WGP paste at 72 h. Freeze-dried residues were fractured into particles with a size of less than 1 mm. Before the SEM analysis, the sample was coated with gold to enhance its conductivity. The SEM was operated at an accelerating voltage of 20 kV.

Mercury intrusion porosimetry (MIP, Micromeritics AutoPore IV 9500) was used to test the pore size distribution of the cement with and without ultra-fine WGP. The paste samples used in the analysis were fractured particles less than 1 mm and soaked in isopropanol to stop the hydration, followed by being dried at 40 °C in a vacuum oven.

2.8 Characterisation of hydration products

To characterise the hydration product of cement paste incorporating ultra-fine WGP, thermogravimetric analysis (TG) was performed. The freeze-dried paste samples were ground into powder before the measurement. The powdered specimens were characterised using Rigaku Thermo Plus EVO2 by heating from 30 °C to 1000 °C at a 10 °C/min rate in an N_2 environment.

X-ray diffraction (XRD, Rigaku SmartLab) was used to compare the crystalline composition in the cement pastes with and without ultra-fine WGP. The ground paste samples, less than 45 μm, were analysed with a parallel beam mode at 45 kV and 200 mA with a CuKα radiation. The freeze-dried samples in Section 0 were co-ground with 10 % of corundum by mass (10 wt%) and then scanned by Rigaku SmartLab 9 kW from 5° to 70° 2θ at a speed of 2.5°/min with a 0.02° step size. Using the Rietveld method, quantitative X-ray Diffraction (QXRD) was conducted to quantify the evolution of various phases in the pastes.

A JEOL ECZ 500 MHZ solid-state nuclear magnetic resonance (NMR) spectrometer with a 7-mm CP/MAS probe using a 4 kHz spinning rate, 98.4 MHz resonance frequency and 20 s relaxation delay was used for the analysis. The paste samples used in the analysis were freeze-dried for 1 h and ground to less than 45 μm. The resulting spectra were deconvoluted and analysed according to Q^n classification [52] (where Q refers to silica tetrahedra (SiO_4), and n refers to different types of silica tetrahedra) to obtain the mean chain length (MCL) and polymerisation degree (PD). Equations (4) and (5) are used to calculate MCL and PD according to a previous study [53].

$$MCL = 2 \times (Q^1 + Q^2) / Q^1 \quad (4)$$

$$PD = Q^2 / Q^1 \quad (5)$$

3. Results

3.1 Physicochemical properties of the prepared ultra-fine WG

Fig. 4 shows the particle size distributions of the ultra-fine WGP. The particle size of the ultra-fine WGP ranged between 300 and 700 nm with a D_{50} of 500 nm. The particle size distribution is similar to that of SF, as the D_{50} of the SF had been reported to range from 100 nm to 300 nm [54].

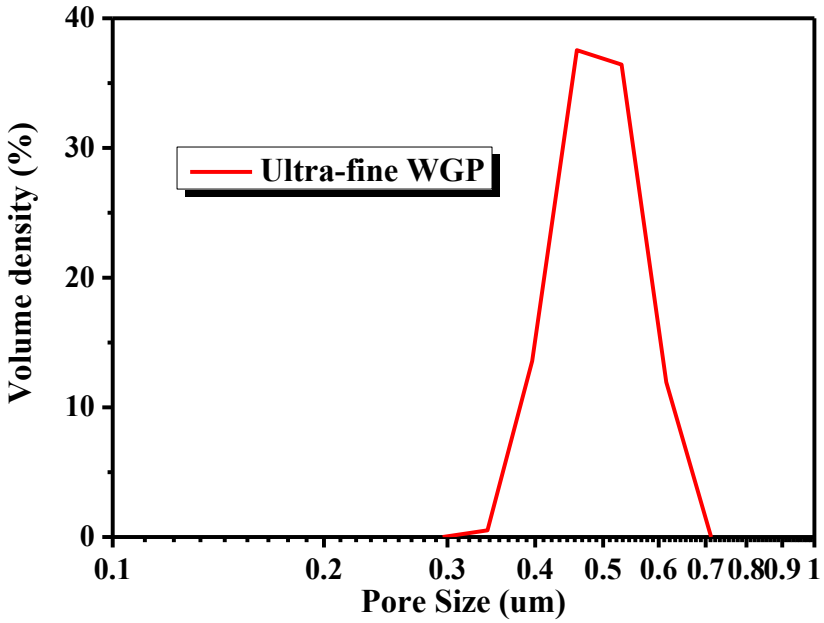

Fig. 4 Particle size distributions of ultra-fine WGP

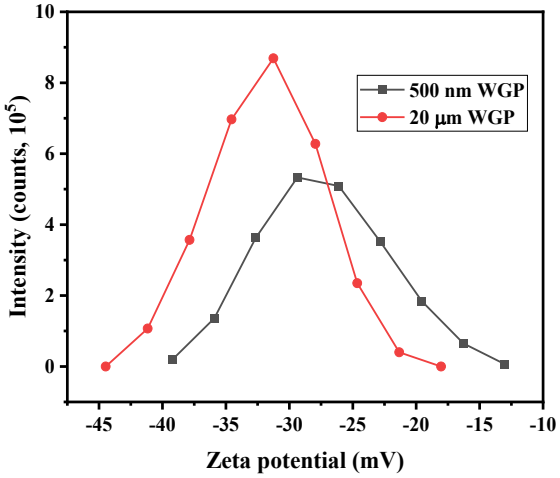

Fig. 5 Zeta potential of ultra-fine WGP

The zeta potential of the ultra-fine WGP shown in Fig. 5 was -28.7 mV, much higher than the micro-size WGP (WGP with D_{50} = 18.6 μm, -31.4 mV). Thus, it can be concluded that the wet-grinding process changed the surface characteristics of WG, which might be attributed to the removal of soluble ions during the wet-grinding process. In addition, the morphologies of ultra-fine WGP (Fig. *6*) also confirmed the change in the surface characteristics of WG. The flocculation observed in Fig. *6* resulted from the lower magnitude of zeta potential (within -30 mV and +30 mV), leading to less repulsive force between the WG particles against van der Waals's attractive forces [55].

Compared with other conventional SCMs, the magnitude of the zeta potential of the ultra-fine WGP was much higher. The previous study reported that the zeta potential of GGBS, FA and SF was -2 mV, 0 mV and -2 mV, respectively [56]. The more negative zeta potential could result in better flowability due to the repulsive force between the particles [15]. Therefore, incorporating ultra-fine WGP might render better workability than conventional SCMs even though the magnitude of the zeta potential was reduced.

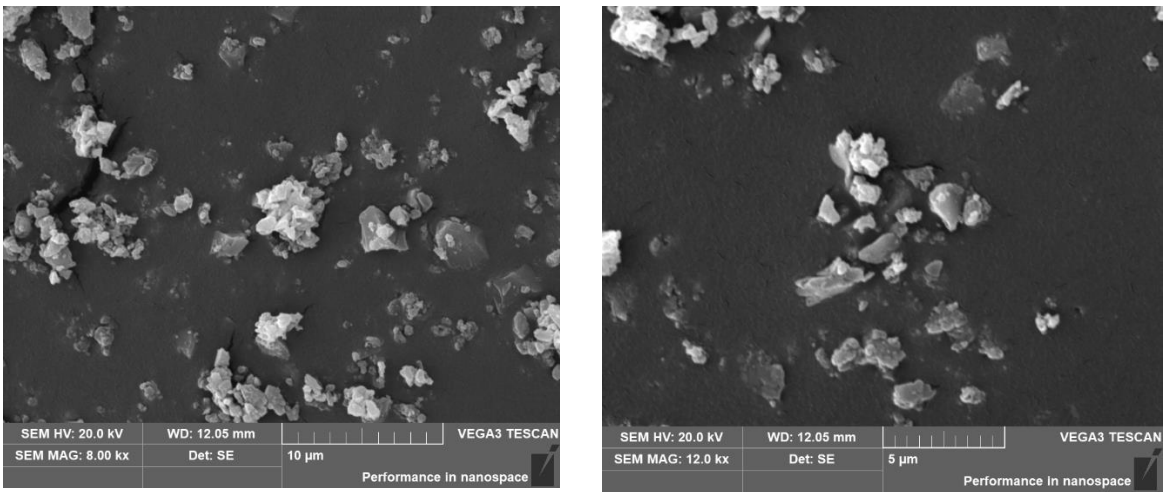

Fig. 6 Morphologies of *ultra-fine* WGP

Fig. 7 shows the Na 1s, Si 2p and Ca 2p XPS spectra of WGP before and after wet-grinding. Firstly, the peak associated with Na 1s (Fig. 7a) right shifted from 1071.8 to 1071.6 with a decreased intensity. The intensity was associated with the quantity of the corresponding atom

on the surface of the materials [57]. The decreased intensity in Na 1s could be attributed to the Na^+ leaching into the water after wet-grinding. The Si 2p spectra (Fig. 7b) also showed a right-shift in binding energy in the ultra-fine WGP, from 102.60 eV to 102.66 eV, but with a widened peak. For the Ca 2p spectrum, the peak was left-shifted from 347.3 eV to 347.0 eV and broadened after grinding. The result indicated that Na on the WGP surface was reduced while silica and calcium remained on the surface of WGP, resulting in more surface defects for the chemical reaction [58], such as with calcium hydroxide (CH) dissolved from cement. The ultra-fine WGP was expected to have higher reactivity.

In summary, ultra-fine WGP was produced from wet grinding. The surface composition and zeta potential of WGP were modified. The modified physicochemical properties of WG might lead to its effects on cement hydration and performance, which are investigated in the following section.

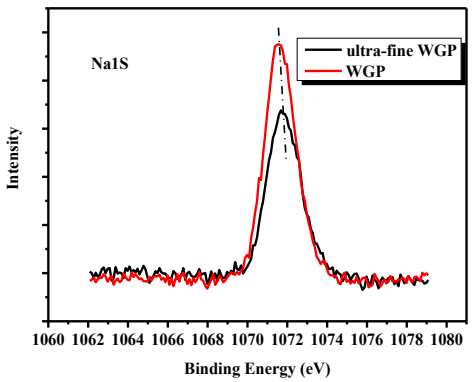

(a) Na1s

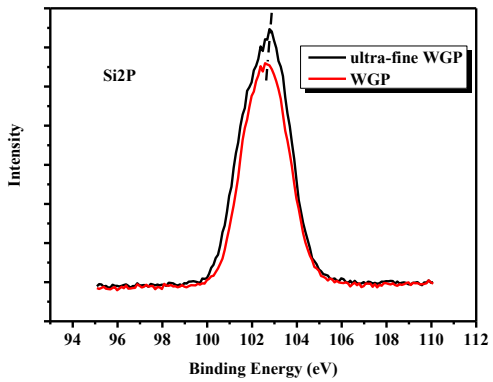

(b) Si2p

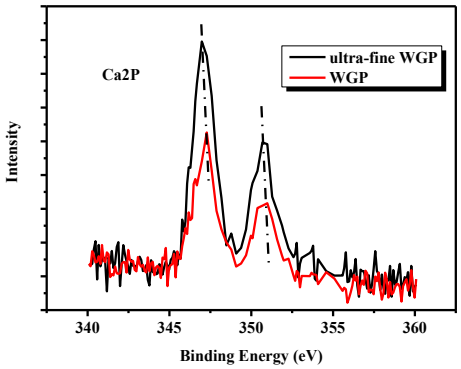

(c) Ca2p

Fig. 7 XPS spectra of WGP for (a) Na1S, (b) Si2P, (c) Ca2P

3.2 Effect of ultra-fine WGP on the fresh properties of cement paste

3.2.1 Slump flow

Fig. 8 shows the slump flow of cement paste prepared with the replacement of ultra-fine WGP. The slump flow decreased from 175 to 150 mm when the replacement by ultra-fine WGP increased from 0 % to 7 %. On the contrary, the incorporation of micro-size WGP was reported to increase the slump flow of cement pastes [59, 60]. Previous study also reported incorporating wet-ground WGP with D_{50} of 900 nm could improve the slump flow [43]. The difference can be attributed to the very high fineness of ultra-fine WGP because the finer particles usually possessed higher surface areas [34].

3.2.2 Setting time

Regarding setting time (Table *4*), the ultra-fine WGP delayed the cement paste's initial and final setting times. The initial and final setting times were delayed by 5 – 10 % and 4 – 8 %, respectively, and the setting time increased with the increasing amount of ultra-fine WGP. However, the delayed setting time was insignificant, similar to previous studies on micron-size WGP replacing 10 % cement [61].

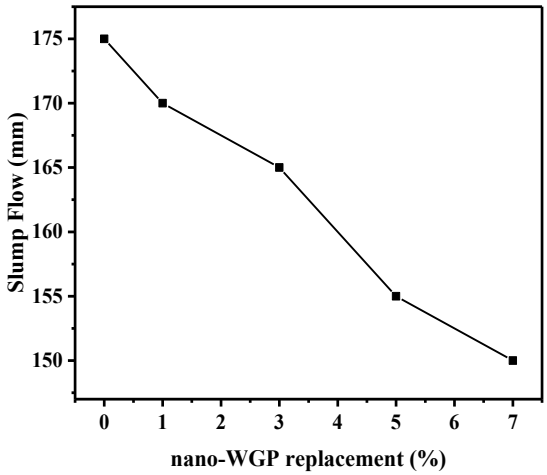

302

303 Fig. 8 Slump flow of cement paste incorporating ultra-fine WGP

304 Table 4 Setting time of cement with different percentages of ultra-fine WGP

	Ref	1%	3%	5%	7%
Initial Setting (min)	195	205	210	210	215
Final Setting (min)	235	245	245	250	255

305

306 *3.3 Mechanical properties*

307 3.3.1 Compressive strength

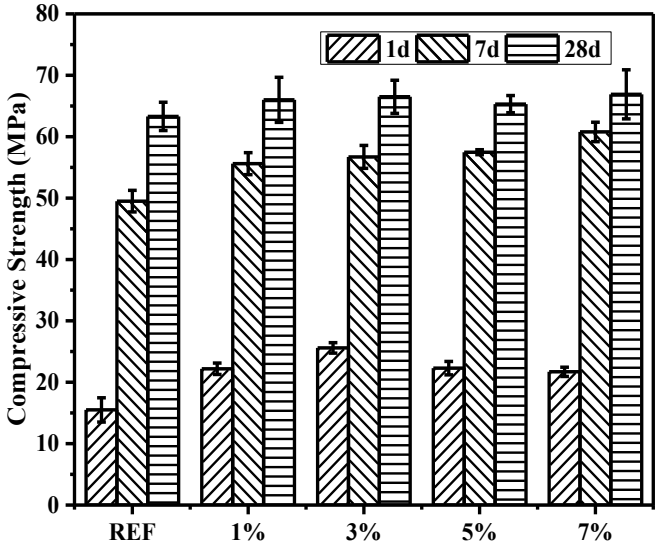

308

Fig. 9 Compressive strength of cement pastes incorporating different percentages of ultra-fine WGP

Fig. 9 shows the compressive strength of cement pastes incorporating different percentages of ultra-fine WGP. Strength improvement was observed in all cement pastes at all testing ages. More significant improvements were observed at an early age. For example, the 1-d strength for the sample containing 3 % ultra-fine WGP had the highest value, 50 % higher than the reference. For the 7-d strength, up to 30 % improvement could be obtained when 7 % of ultra-fine WGP was added. Moreover, a slight improvement (3-5 %) could be observed in the 28-d strength of samples incorporating different amounts of ultra-fine WGP. It can be concluded that the ultra-fine WGP significantly influenced the early-age development of mechanical properties, which would mitigate the adverse effect of conventional SCMs on the early strength.

3.3.2 Micro-mechanical properties

To provide a more comprehensive investigation of the effect of ultra-fine WGP on the early mechanical properties of cement paste, nano-indention analysis was used to quantify the micro-mechanical properties of the hydration products at 72 h. *Fig. 10* illustrates the indentation modulus distribution of the hydration products of the samples prepared with and without 3 % ultra-fine WGP. The results identified three phases: C-S-H with low density (LD) and high density (HD) and unhydrated clinker in the cement paste samples. According to the previous studies, the LD and HD C-S-H had an indentation modulus of 10 – 26 GPa and 25 – 39 GPa and a hardness of 0.4 – 0.8 and 0.8 – 1.25, respectively. [62], while the unhydrated clinker had a higher indentation modulus and hardness of above 93 GPa and 3 GPa, respectively. *Fig. 11* demonstrated the volume percentage of the different phases based on Fig. 10. The LD and HD of C-S-H in REF were 61 % and 7 %, respectively, while LD and HD in 3 % were 7 % and 10 % higher than the REF. In addition, the amount of unhydrated phase in the 3 % ultra-fine WGP decreased from 32 % to 15 %. Therefore, the addition of ultra-fine WGP not only accelerated the cement hydration but also promoted the formation of C-S-H. As a result, a significant strength enhancement (up to 50 %) was observed at 3 d (Fig. *9*).

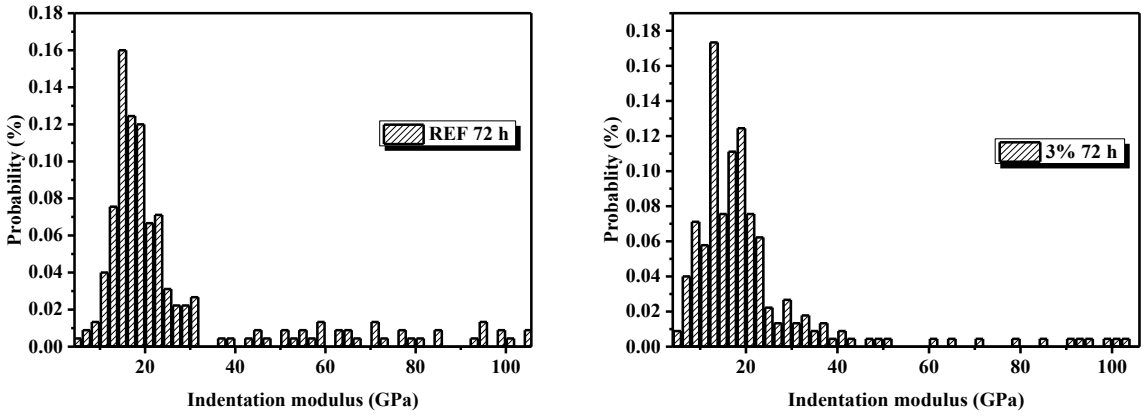

(a) REF 72 h (b) 3% 72 h

335 Fig. 10 Statistical distribution of indentation modulus for cement paste with and without ultra-fine WGP at 3d

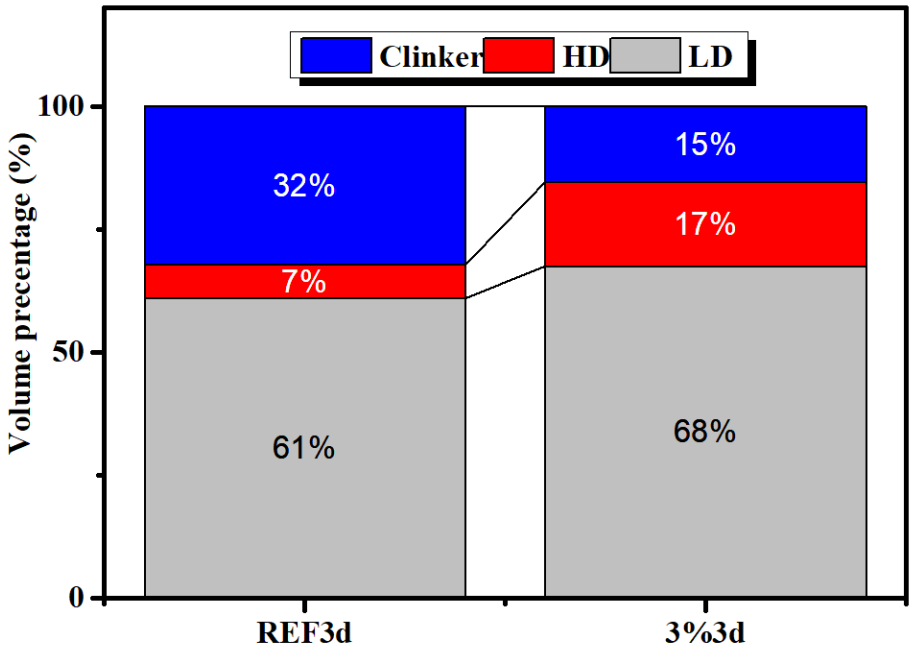

336

337 Fig. 11 Volume percentages of different phases in cement pastes prepared with and without ultra-fine WGP

338 *3.4 Effect of ultra-fine WGP on the pore structure*

339 Fig. *12* illustrates the pore structure of the cement pastes prepared with and without ultra-fine
340 WGP at 8 h and 3 d. To quantitatively characterise the pore-refining effect by incorporating
341 ultra-fine WGP in the cement paste, a classification of pore structure was suggested at three
342 ranges: 4.5 - 50 nm (mesopores), 50 - 100 nm (medium capillary pores), and >100 nm (large
343 capillary pores). Table *5* illustrates the proportion of these pores at 8 h and 72 h. At 8 h, with

the ultra-fine WGP, the large capillary pores of the paste were 63.2 %, 5.9 % lower than the reference, whereas the proportion of medium capillary pores and mesopores was 0.3 % and 5.6 % higher, respectively. At the same time, the cumulative pore volume of ultra-fine WGP cement paste was 0.272 mL/g, comparable to that of the reference (0.265 mL/g). In addition, a similar trend was also observed in the 3-d samples. At 72 h, the volume of large pores was fewer with ultra-fine WGP, approximately 5.9 % lower than the REF. The medium capillary pores and mesopores were also 2.1 % and 3.7 % higher, respectively, in samples prepared with ultra-fine WGP. The 72-h cumulative pore volume was also similar in both samples, approximately 0.160 mL/g. Therefore, incorporating a small amount of ultra-fine WGP had a limited effect on the total porosity of the cement paste but refined the pore structure at an early age.

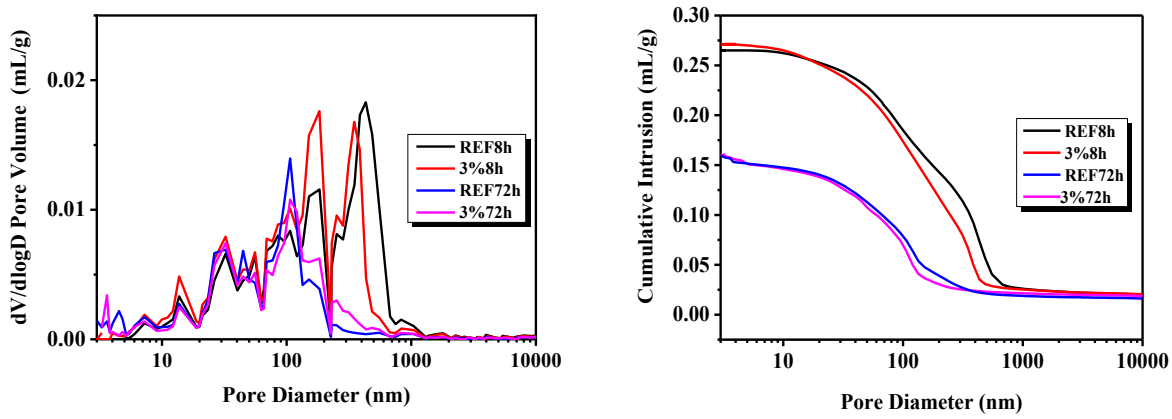

(a) (b)

Fig. 12 (a) Pore volume distributions and (b) cumulative pore volumes of cement pastes prepared with and without ultra-fine WGP

Table 5 Pore size proportion of cement paste at 8 h and 72h

Pore proportion (%)	mesopores	medium capillary pores	large capillary pores
REF 8h	14.0	16.9	69.1
3% 8h	19.6	17.2	63.2
REF 72h	29.1	21.3	49.7
3% 72h	32.8	23.4	43.8

359 *3.5 Evolution of hydration product in cement paste incorporating WGP*

360 3.5.1 Thermogravimetric analysis

361 To explore the acceleration effect of WGP at an early age, the hydration of the samples
362 prepared with and without WG was stopped at 1.5 h, 8 h, 24 h and 72 h, and a TG test was
363 conducted. Fig. 13 compares the TG and DTG curves of the cement paste prepared with and
364 without ultra-fine WGP. The DTG curve (Fig. 13a) illustrates several peaks of mass loss. The
365 first peak around 100 to 200 °C was attributed to the dehydration of free water and chemically
366 bound water of hydrates such as C-S-H and AFt [63, 64]. Another peak around 450 °C was
367 attributed to the dehydroxylation of $Ca(OH)_2$ [65]. The cement paste incorporating ultra-fine
368 WGP had wider C-S-H and CH peaks than the REF before 2 d, while the intensity of the peak
369 corresponding to CH was lower than that of the reference sample at 72 h. The quantity of CH
370 could be calculated based on the DTG curves, and the results showed that there was 3.85 %
371 CH in the ultra-fine WGP samples, which was 4 times higher than that in the reference sample
372 (0.93 %) at 1.5 h CH. At 24 h, the CH mass loss was also 0.62 % higher than the REF (9.88 %)
373 when ultra-fine WGP (10.5 %) was incorporated. Therefore, at a very early age (<3 d), the
374 presence of ultra-fine WGP promoted the formation of hydration products, including CH, C-
375 S-H and ettringite, which was attributed to the acceleration effect of WGP on cement hydration.
376 However, the WGP also has pozzolanic reactivity that could participate in the cement hydration
377 and consume some CH. As a result, the CH was reduced at 72 h, and the ultra-fine WGP sample
378 had a lower CH content than the reference sample at 72 h.

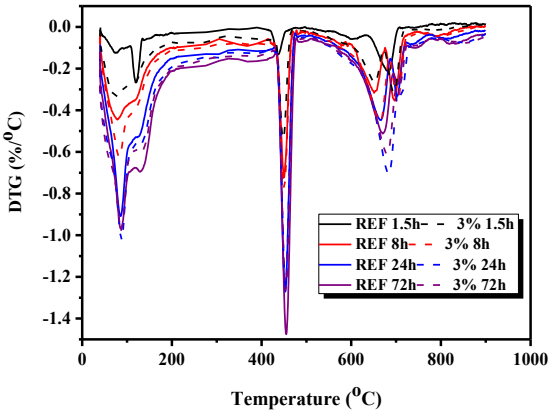

(a)

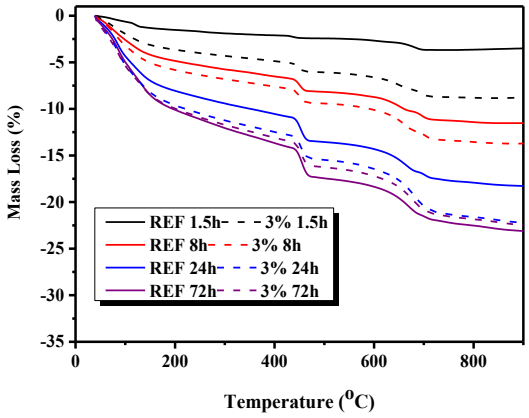

(b)

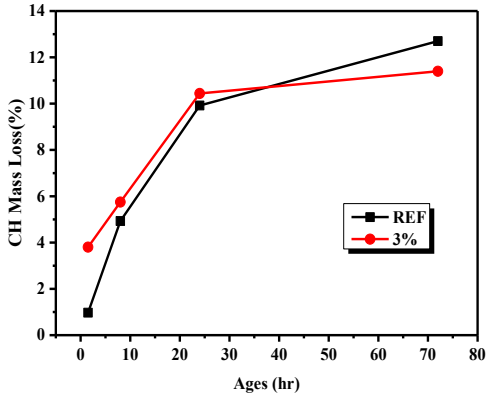

(c)

379 Fig. 13 a) TG curve, b) DTG curve and c) mass loss of CH of cement pastes prepared with and without ultra-fine WGP

380 3.5.2 ^{29}Si Solid-state NMR

381 ^{29}Si MAS-NMR analysis was conducted to analyse the structure of the silicate phases in the

382 cement paste prepared with and without ultra-fine WGP, and the results are shown in Fig. *14*.

383 Three prominent peaks were observed in all the ^{29}Si MAS-NMR spectra, which were Q^0 at -72

384 ppm, Q^1 at -81 ppm and Q^2 at -86 ppm, respectively. The Q^n indicated a different state of SiO_4

385 in the specimens: Q^0 represented the SiO_4 in cement, Q^1 represented the SiO_4 for bridging in

386 C-S-H, and Q^2 represented the SiO_4 at the end-chain of C-S-H and SiO_4 [63]. The peak of Q^n

387 was quantified after deconvolution. At 8 h, the Q^0 of ultra-fine WGP samples was 68.6 %, 6.6

388 % lower than the REF. However, the Q^1 and Q^2 peaks of the ultra-fine WGP samples were

increased to 24.8 % and 6.53 % from 20.3 % and 4.4 %, respectively. A similar trend was observed in the 3-d samples. The Q^0 of ultra-fine WGP samples was 48.3 %, 9.3 % lower than the REF. The Q^1 (37.05 %) and Q^2 (14.6 %) were also higher in the ultra-fine WGP samples, 5.35 % and 4 % higher than the REF, respectively. The results indicated that the amount of hydration products in the cement paste was increased after adding the ultra-fine WGP.

The MCL and PD of C-S-H were calculated according to equations (4) and (5), and the results are shown in Table *6*. The MCL of the reference sample was 2.43 at 8 h, but it increased to 2.53 after adding ultra-fine WGP. The MCL was also increased from 2.67 to 2.79 at 3 d because of the ultra-fine WGP incorporation. Thus, adding a small amount of ultra-fine WGP promoted cement hydration and increased the MCL of C-S-H. Similarly, adding 3 % ultra-fine WGP led to 20 % higher PD than the reference at all the tested ages, indicating that the connectivity ratio of the hydrate species was significantly increased. The result might suggest that the ultra-fine WGP particles could provide nucleation sites for C-S-H precipitation, resulting in early C-S-H polymerisation. Generally, the formation of hydrates with very long chains correlated with the increase in compressive strength of concrete and could hinder the development of micro-cracks [66]. These might be one of the reasons contributing to the significantly enhanced compressive strength at a very early age.

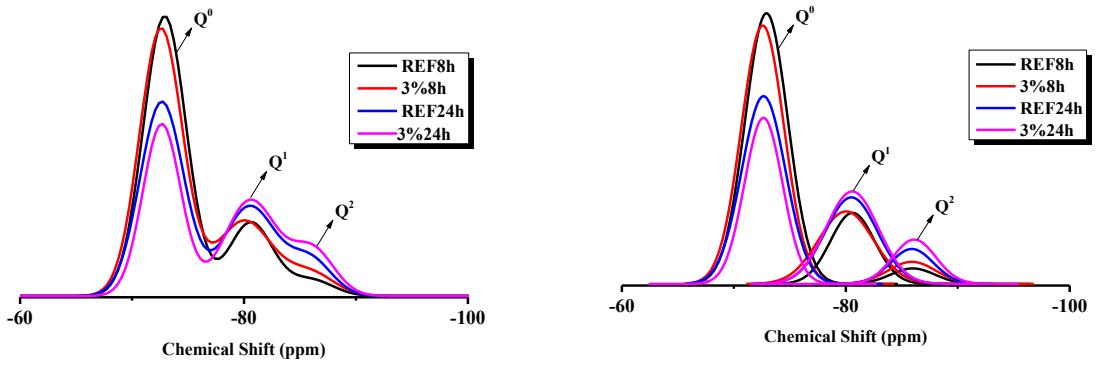

(a) ^{29}Si MAS-NMR spectrum (b) Deconvoluted peaks

Fig. 14 ^{29}Si MAS-NMR spectra and deconvoluted peaks of cement pastes incorporating ultra-fine WGP; Note: R: reference

Table 6 MCL & PD of C-S-H in cement pastes prepared with and without ultra-fine WGP based on ^{29}Si MAS-NMR

	Q^n/%				
	Q^0	Q^1	Q^2	MCL	PD
REF 8h	75.2	20.3	4.4	2.43	0.22
3% 8h	68.6	24.8	6.53	2.53	0.26
REF 24h	57.6	31.7	10.6	2.67	0.33
3% 24h	48.3	37.05	14.6	2.79	0.39

3.6 Hydration kinetics

3.6.1 Heat of hydration

Fig. 15 shows the hydration heat evolution profiles of the cement pastes prepared with and without ultra-fine WGP up to 72 h. As shown in Fig. 15 and b, all samples incorporating ultra-fine WGP released more significant amounts of heat than the reference sample at an early age (<30 min). Regarding the first heat evolution peak, its occurrence was approximately 2 h earlier in the samples prepared with 5 % (7.4 h) and 7 % (7.6 h) ultra-fine WGP, while 0.4 h earlier with 3 % ultra-fine WGP (8.9 h) than the REF (9.3 h). The first peak (peak 1) of samples prepared with 5 % ultra-fine WGP (2.88 mW/g) was also 0.08 mW/g higher than the REF, while 3 % and 7 % were 0.06 and 0.05 mW/g lower than the REF. Peak 2, associated with the depletion of gypsum and ettringite formation [67], of 5 % and 7 % was observed 2 h earlier than the REF, indicating accelerated C_3A hydration [68]. The AFm formation (peak 3), associated with transformation from AFt to AFm, also occurred more than 7 h earlier in 5 % and 7 % than the REF and 1 h earlier in 3 %. Besides, the difference in cumulative heat release between cement pastes prepared with or without ultra-fine WGP was insignificant except for the 5 % ultra-fine WGP sample. The observation was related to the enhancement of 3-d strength. Overall, the ultra-fine WGP accelerated the cement hydration with a low dosage. The result

was observed in the previous literature and was attributed to the increased reactivity in ultra-fine WGP or seeding effect [43]. It should be noted that five stages of hydration were selected for further investigation, including the beginning of the dormant period (1.5 h), the occurrence of the second and third peaks (8 h and 10 h, respectively), the end of the deceleration period (24 h) and densification (72 h) [69].

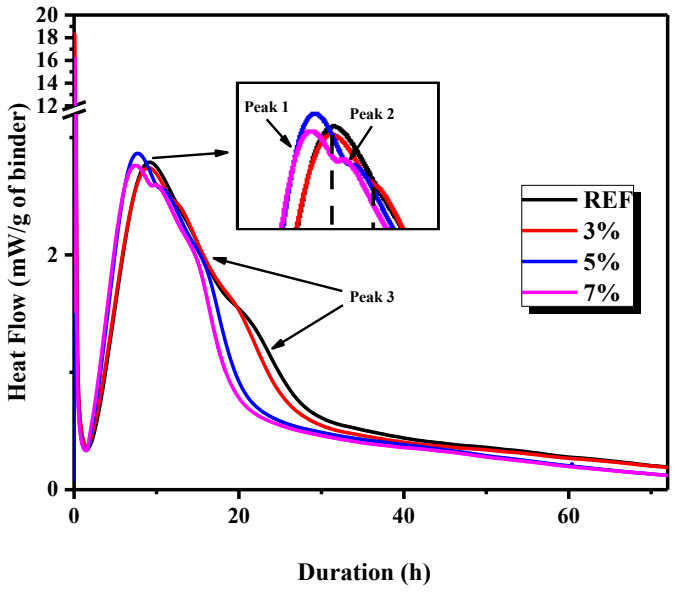

(a)

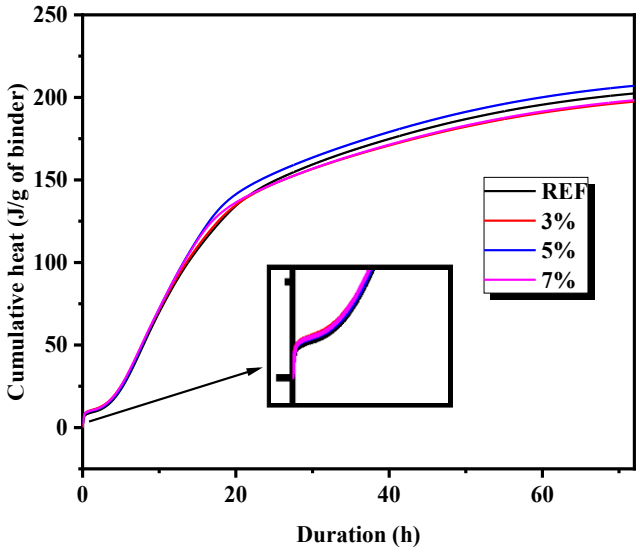

(b)

Fig. 15 (a) Heat Flow and (b) Cumulative heat of cement pastes prepared with ultra-fine WGP

3.6.2 Effect of ultra-fine WG on pore solution

Fig. 16 demonstrates the evolution of the cation and anion concentrations in the pore solution of the cement paste. The concentration of Al^{3+} (Fig. *16*a) in the ultra-fine WGP paste at 1.5 h was 42.8 ppm, approximately 10 % higher than the REF. The higher Al^{3+} concentration in the pore solution might be related to the enhanced dissolution of C_3A when ultra-fine WGP was present [70], which is consistent with the observation in the calorimeter result. After 10 h, the Al^{3+} concentration in the ultra-fine WGP paste rapidly declined and remained steady at approximately 38.0 ppm, while the concentration of the REF reached a maximum value at 10 h and then decreased gradually. Fig. 16 b and c showed that the initial concentrations of Na^+ and K^+ were lower in the ultra-fine WGP paste. The result might be attributed to the high initial Al^{3+} concentration suppressing the initial release of Na^+ and K^+ to balance the ion charge in the pore solution. For the REF, the Na^+ concentration was continuously reduced after 10 h. In contrast, the Na^+ concentration of the ultra-fine WGP cement paste began to increase rapidly, reaching 100 ppm at 72 h. The increased Na^+ concentration after 10 h was attributed to the dissolution of WGP [70, 71], which resulted in accelerated cement hydration and early strength development [68]. Previous studies showed that hydration kinetics was associated with ion concentration, temperature and pressure [72, 73]. Unlike Na^+, the dissolution of K^+ was hindered by ultra-fine WGP at the initial age, where its concentration was 720 ppm at 1.5 h, which was only half of the reference (1400 ppm). The K^+ concentration of the pore solution in the samples incorporating ultra-fine WGP increased rapidly between 1.5 h and 10 h, while the K^+ concentration of the REF showed a decreasing trend. Similar K^+ concentrations could be observed after this initial stage.

Apart from K^+, the high Na^+ concentration in the ultra-fine WGP cement paste also suppressed Ca^{2+} dissolution (Fig. *16* d), facilitating the release of OH^- (Fig. *16* e) [74]. The Ca^{2+} concentration decreased rapidly in both samples but became stable at approximately 200 ppm after 24 h. However, the Ca^{2+} concentration of the samples incorporating ultra-fine WGP was 20 ppm lower than the reference. The suppressed Ca^{2+} concentration was attributed to the reduced Ca(OH)2 solubility when higher alkalinity was present in the samples prepared with ultra-fine WGP [68]. In addition, the rapid decrease of Ca^{2+} concentration was related to the enhanced formation of C-S-H. The higher alkalinity was related to incorporating ultra-fine WGP, forming more C-S-H layers [68]. Another reason for the reduction of Ca^{2+} concentration in the ultra-fine WGP incorporated samples could be attributed to the pozzolanic reaction of ultra-fine WGP. The OH^-concentration was also slightly modified due to the incorporation of ultra-fine WGP [75]. The OH^-concentration was similar in both samples before 12 h but became approximately 100 ppm higher in the samples prepared with ultra-fine WGP at 72 h. The higher OH^-concentration was attributed to the higher Na^+ concentration, resulting in ettringite precipitation and OH^-leaching into the pore solution [68]. In summary, a small amount of ultra-fine WGP addition modified the ion concentrations in the pore solution, which also modified the hydration kinetics of the cement paste.

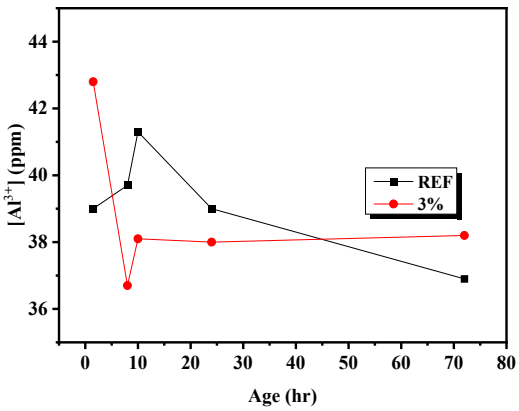

(a)

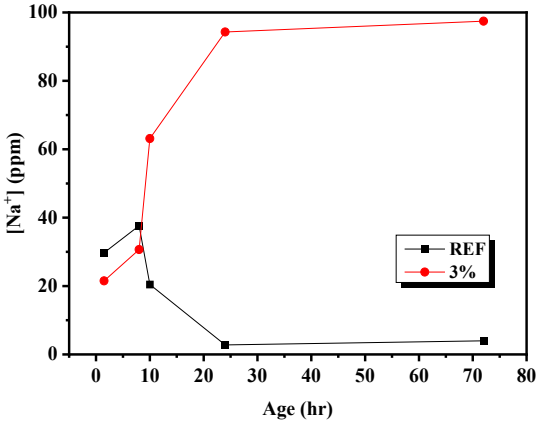

(b)

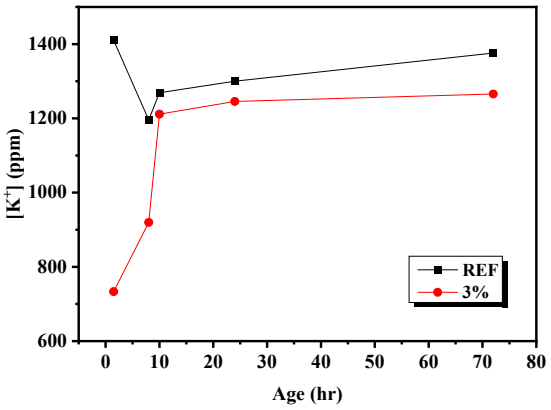

(c)

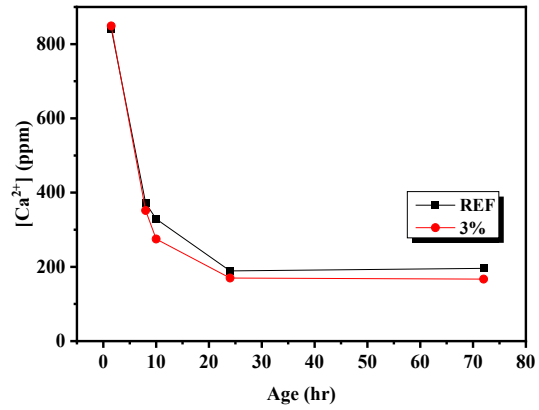

(d)

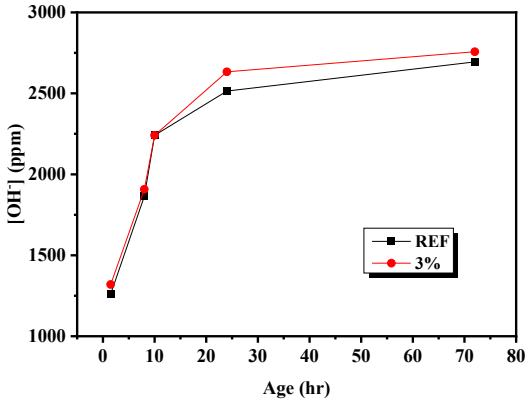

(e)

472 Fig. 16 Evolution of the concentrations of a) Al^{3+}, b) Ca^{2+}, c) Na^{+}, d) K^{+}, e) OH^{-} in cement pastes prepared with and without
473 ultra-fine WGP

4. Discussion

4.1 Acceleration mechanism of OPC hydration

The wet-grinding process might lead to the leaching of ions, such as Na, Al and Si, from WGP into a solution. Meanwhile, the mechanical milling produced defects on the surface of WGP, leading to enhanced reactivity with cement [58]. In section 3.5.2, the result showed that a small amount of ultra-fine WGP modified the ion concentration of the pore solution. The change in pore solution would also influence the hydration kinetics, such as the dissolution and precipitation of hydration products, including ettringite, CH and C-S-H. Therefore, the SI of ettringite, CH and C-S-H (*Fig. 17*) were used to analyse the trend of dissolution/precipitation of the hydration products. The SI of ettringite (*Fig. 17*a) shows that the sample prepared with ultra-fine WGP had a slightly higher SI at 1.5 h than the REF. The ettringite SI of both samples then rapidly decreased and became steady after 24 h. The ettringite SI was consistent with the observation in the heat flow test (section 3.6.1), which suggested that incorporating ultra-fine WGP provided adequate aluminium in the pore solution to promote the formation of AFt. The CH SI (*Fig. 17*b) of the samples prepared with ultra-fine WGP was also higher in all testing ages than in the reference. Adding ultra-fine WGP had the highest CH SI at a very early age, while the reference peak was recorded at 10 h. In addition, the sample with ultra-fine WGP had a higher C-S-H SI before 72 h. Therefore, adding ultra-fine WGP also promoted the precipitation of CH and C-S-H at a very early age. The result suggested that the dissolution of ultra-fine WGP increased Ca, Al and Si ions in the pore solution, which accelerated the hydration rate of cement.

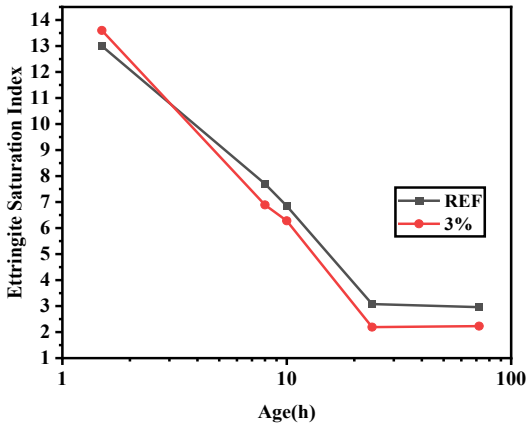

(a)

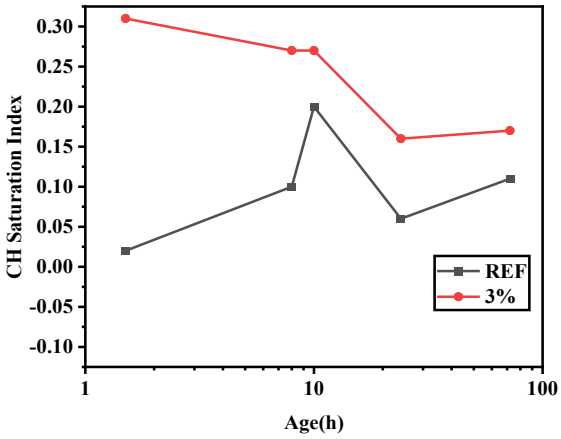

(b)

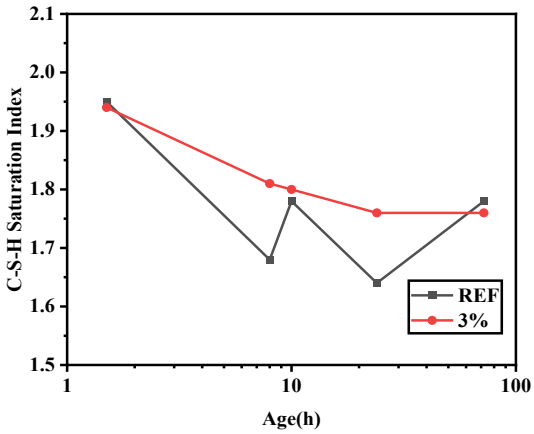

(c)

Fig. 17 Saturation index of (a) ettringite (b) CH (c) C-S-H

4.2 Role of the physicochemical properties of ultra-fine WGP on the performance of OPC

According to the above results, incorporating the ultra-fine WGP accelerated cement hydration significantly enhanced compressive strength development. This effect would be closely related to the physicochemical properties of WGP prepared by wet grinding. The relations between the physicochemical properties of WGP and the evolution of performance are discussed as follows:

Firstly, the enhanced early hydration promoted by the nucleation effect was achieved using the submicron-sized WGP [76]. In this study, ultra-fine WGP with a D_{50} of 500 nm was produced

through wet grinding, which was used as nucleation seeds to accelerate the hydration of clinkers.

However, unlike other nanoparticles, such as nano-SiO_2 and C-S-H, the ultra-fine WGP could also enhance the dissolution of alkali ions into the pore solution due to the defects on the surface produced from wet-grinding [58]. The high alkalinity environment could facilitate the precipitation of ettringite and the formation of C-S-H, leading to better early strength development [68].

As an SCM, ultra-fine WGP could participate in pozzolanic reactions with cement at an early age to form gel products, which are different from micron-sized WGP. Generally, micron-size WGP could retard the hydration and mainly contribute to later strength [43]. However, the wet grinding process could produce defects on the surface of WG [58], which provided reactive sites for the reaction with CH, leading to higher pozzolanic reactivity. The early reduced Ca^{2+} concentration might indicate that CH was consumed and participated in the pozzolanic reaction at an early age. In addition, the gel products produced from ultra-fine WG-cement consisted of more HD C-S-H (as shown in Fig. *11*), which was associated with the refined pore structure in this study. The lower porosity observed in the cement paste with ultra-fine WGP could explain the higher 1-d compressive strength. Furthermore, the modified surface of ultra-fine WG was also associated with longer MCL and higher polymerisation of C-S-H. The ultra-fine WG might facilitate the dissolution of Si ions, which participated in the polymerisation of C-S-H. Overall, the ultra-fine WG via the above mechanisms could, therefore, serve as an early-age accelerator, compensating for the disadvantages of using micron-size WGP in cement-based materials, such as low strength at an early and later age.

4.3 Innovation significance and recommendation for future work

The significance of this study could be divided into environmental and applicable aspects. Firstly, part of WG is disposed of at a landfill as waste daily. Broadening the application of

WG could consume WG as a resource and reduce the accumulation of WG at landfills. Wet-grinding of WG is a less costly approach to producing reactive cementitious materials, which enhances the feasibility and applicability of advanced construction materials with large volumes of costly binders, such as ultra-high-performance concrete (UHPC). Ultra-fine WG was aimed to replace costly cement or other high-quality SCMs, such as GGBS and SF.

This study mainly focuses on the physicochemical properties of ultra-fine WGP and proposes the mechanism of ultra-fine WGP in cement hydration, mechanical performance, and microstructure. Therefore, more work could be conducted to validate the feasibility of using ultra-fine WGP in concrete in the future. While the higher reactivity was observed, a comparison to other conventional SCMs, especially silica fume, could be carried out to demonstrate the merits of ultra-fine WGP and the possibility of replacing conventional SCMs. Moreover, using WG in concrete could raise concerns about durability performance, such as ASR and shrinkage. More investigation on the durability of concrete should be suggested. Last but not least, some works could also focus on the effects of incorporating high-volume ultra-fine WG on the long-term performance of concrete.

5. Conclusion

This study investigated the effect of wet grinding on the physicochemical properties of WGP and the effect of incorporating the wet grinding of WGP on the early hydration kinetics, mechanical performance, and microstructure of cement pastes. The conclusion of this study is summarised as follows:

1. Through wet-grinding, ultra-fine WGP with D_{50} of 500 nm was produced with a modified surface composition and zeta potential.
2. Ultra-fine WGP significantly influences the early-age development of the mechanical properties of the cement paste. Incorporating ultra-fine WGP increased 1-d, 7-d and 28-d

compressive strength by 50 %, 30 %, and 10 %, respectively. Therefore, incorporating ultra-fine WGP would mitigate the adverse effect of conventional SCMs on early strength.

3. A small amount (3 %) of ultra-fine WGP incorporation increased the alkaline ion concentration and pH in the pore solution of the cement paste. The higher alkalinity environment enhanced the precipitation of ettringite and the formation of C-S-H, leading to better early strength development.
4. Ultra-fine WGP can be characterised as a new material with multiple effects on nucleation, hydration kinetics, mechanical performance and microstructure of cement pastes. It could be an alternative to substitute reactive but costly SCMs.

6. Acknowledgement

The study was supported by a grant from the Research Grants Council of the Hong Kong Special Administrative Region, China (Project No. T22-502/18-R) and the Green Tech Fund of the Hong Kong Special Administrative Region, China (Project No. K-ZB5B). The authors also gratefully acknowledge the support of the University Research Facility on Chemical and Environmental Analysis (UCEA) of PolyU.

Reference

[1] A. Olabi, M.A. Abdelkareem, Renewable energy and climate change, Renewable and Sustainable Energy Reviews 158 (2022) 112111.

[2] Global Cement and Concrete Association, Cement and Concrerte Around The World, 2022. https://gccassociation.org/concretefuture/cement-concrete-around-the-world/. (Accessed 11 22 2022).

[3] Z. Cao, R.J. Myers, R.C. Lupton, H. Duan, R. Sacchi, N. Zhou, T. Reed Miller, J.M. Cullen, Q. Ge, G. Liu, The sponge effect and carbon emission mitigation potentials of the global cement cycle, Nature communications 11(1) (2020) 3777.

[4] J. Rocha, R. Toledo Filho, N. Cayo-Chileno, Sustainable alternatives to CO2 reduction in the cement industry: A short review, Materials Today: Proceedings (2022).

[5] S.A. Miller, A. Horvath, P.J. Monteiro, Readily implementable techniques can cut annual CO2 emissions from the production of concrete by over 20%, Environmental Research Letters 11(7) (2016) 074029.

[6] Environment UN, K.L. Scrivener, V.M. John, E.M. Gartner, Eco-efficient cements: Potential economically viable solutions for a low-CO2 cement-based materials industry, Cement and Concrete Research 114 (2018) 2-26.

[7] M. Manjunatha, S. Preethi, H. Mounika, K. Niveditha, Life cycle assessment (LCA) of concrete prepared with sustainable cement-based materials, Materials Today: Proceedings 47 (2021) 3637-3644.

[8] M.A. Sanjuán, C. Argiz, P. Mora, A. Zaragoza, Carbon dioxide uptake in the roadmap 2050 of the Spanish cement industry, Energies 13(13) (2020) 3452.

[9] C.D. Dinga, Z. Wen, China's green deal: Can China's cement industry achieve carbon neutral emissions by 2060?, Renewable and Sustainable Energy Reviews (2021) 111931.

[10] X. Cao, Z. Wen, X. Zhao, Y. Wang, H. Zhang, Quantitative assessment of energy conservation and emission reduction effects of nationwide industrial symbiosis in China, Science of the Total Environment 717 (2020) 137114.

[11] M.C. Juenger, R. Snellings, S.A. Bernal, Supplementary cementitious materials: New sources, characterization, and performance insights, Cement and Concrete Research 122 (2019) 257-273.

[12] M.U. Hossain, C.S. Poon, Y.H. Dong, D. Xuan, Evaluation of environmental impact distribution methods for supplementary cementitious materials, Renewable and Sustainable Energy Reviews 82 (2018) 597-608.

[13] M.U. Hossain, J.-C. Liu, D. Xuan, S.T. Ng, H. Ye, S.J. Abdulla, Designing sustainable concrete mixes with potentially alternative binder systems: Multicriteria decision making process, Journal of Building Engineering 45 (2022) 103587.

[14] C. Tan, X. Yu, Y. Guan, A technology-driven pathway to net-zero carbon emissions for China's cement industry, Applied Energy 325 (2022) 119804.

[15] J.-X. Lu, P. Shen, Y. Zhang, H. Zheng, Y. Sun, C.S. Poon, Early-age and microstructural properties of glass powder blended cement paste: Improvement by seawater, Cement and Concrete Composites 122 (2021) 104165.

[16] United States Environmental Protection Agency, Facts and Figures about Materials, Waste and Recycling - Glass: Material-Specific Data, 2021. https://www.epa.gov/facts-and-figures-about-materials-waste-and-recycling/glass-material-specific-data. (Accessed 09/16 2022).

[17] J.-X. Lu, X. Yan, P. He, C.S. Poon, Sustainable design of pervious concrete using waste glass and recycled concrete aggregate, Journal of cleaner production 234 (2019) 1102-1112.

[18] Y. Jiang, T.-C. Ling, K.H. Mo, C. Shi, A critical review of waste glass powder–Multiple roles of utilization in cement-based materials and construction products, Journal of environmental management 242 (2019) 440-449.

[19] M.N.N. Khan, A.K. Saha, P.K. Sarker, Reuse of waste glass as a supplementary binder and aggregate for sustainable cement-based construction materials: A review, Journal of Building Engineering 28 (2020) 101052.
[20] K. Sun, H.A. Ali, D. Xuan, C.S. Poon, Sulfuric acid resistance behaviour of alkali-activated slag and waste glass powder blended precursors, Cement and Concrete Composites 145 (2024) 105319.
[21] Y. Du, W. Yang, Y. Ge, S. Wang, P. Liu, Thermal conductivity of cement paste containing waste glass powder, metakaolin and limestone filler as supplementary cementitious material, Journal of Cleaner Production 287 (2021) 125018.
[22] H. Du, K.H. Tan, Properties of high volume glass powder concrete, Cement and concrete composites 75 (2017) 22-29.
[23] S. Yang, J.-X. Lu, C.S. Poon, Recycling of waste glass in dry-mixed concrete blocks: Evaluation of alkali-silica reaction (ASR) by accelerated laboratory tests and long-term field monitoring, Construction and Building Materials 262 (2020) 120865.
[24] Z. Shi, G. Geng, A. Leemann, B. Lothenbach, Synthesis, characterization, and water uptake property of alkali-silica reaction products, Cement and Concrete Research 121 (2019) 58-71.
[25] H. Elaqra, R. Rustom, Effect of using glass powder as cement replacement on rheological and mechanical properties of cement paste, Construction and Building Materials 179 (2018) 326-335.
[26] J.-x. Lu, Z.-h. Duan, C.S. Poon, Fresh properties of cement pastes or mortars incorporating waste glass powder and cullet, Construction and Building Materials 131 (2017) 793-799.
[27] O.Y. Bayraktar, Possibilities of disposing silica fume and waste glass powder, which are environmental wastes, by using as a substitute for Portland cement, Environmental Science and Pollution Research 28(13) (2021) 16843-16854.
[28] Y. Cai, D. Xuan, C.S. Poon, Effects of nano-SiO2 and glass powder on mitigating alkali-silica reaction of cement glass mortars, Construction and Building Materials 201 (2019) 295-302.
[29] M.O. Yusuf, K.A.A. Al-Sodani, A.H. AlAteah, M.M. Al-Tholaia, A.A. Adewumi, A.O. Bakare, A.K. Usman, I. Momohjimoh, Performances of the synergy of silica fume and waste glass powder in ternary blended concrete, Applied Sciences 12(13) (2022) 6637.
[30] Q. Li, H. Qiao, A. Li, G. Li, Performance of waste glass powder as a pozzolanic material in blended cement mortar, Construction and Building Materials 324 (2022) 126531.
[31] L.S. Carneiro, T. Iyoda, Behaviour of cement paste with different particle size of recycled glass on ASR and pozzolanic activity, The 15th Southeast Asian Technical University Consortium (SEATUC) Symposium, 2021, pp. 658-663.
[32] S. Sakir, S.N. Raman, M. Safiuddin, A.A. Kaish, A.A. Mutalib, Utilization of by-products and wastes as supplementary cementitious materials in structural mortar for sustainable construction, Sustainability 12(9) (2020) 3888.
[33] J. Ying, T. Yuan, Y. Jin, L. Fan, State of the Art on Waste Glass Powder as Supplementary Cementitious Material, Engineering Science & Technology (2023) 80-94.
[34] K.S. Ahmed, L.R. Rana, Fresh and hardened properties of concrete containing recycled waste glass: A review, Journal of Building Engineering (2023) 106327.
[35] H. Lee, A. Hanif, M. Usman, J. Sim, H. Oh, Performance evaluation of concrete incorporating glass powder and glass sludge wastes as supplementary cementing material, Journal of Cleaner Production 170 (2018) 683-693.
[36] H. Zhu, M. Ma, X. He, Z. Zheng, Y. Su, J. Yang, H. Zhao, Effect of wet-grinding steel slag on the properties of Portland cement: An activated method and rheology analysis, Construction and Building Materials 286 (2021) 122823.

667 [37] S.C. Chelgani, M. Parian, P.S. Parapari, Y. Ghorbani, J. Rosenkranz, A comparative study
668 on the effects of dry and wet grinding on mineral flotation separation–a review, Journal of
669 Materials Research and Technology 8(5) (2019) 5004-5011.
670 [38] Y. Wang, X. He, Y. Su, H. Tan, J. Yang, M. Lan, M. Ma, B. Strnadel, Self-hydration
671 characteristics of ground granulated blast-furnace slag (GGBFS) by wet-grinding treatment,
672 Construction and Building Materials 167 (2018) 96-105.
673 [39] J. Zhang, H. Tan, X. He, W. Yang, X. Deng, Utilization of carbide slag-granulated blast
674 furnace slag system by wet grinding as low carbon cementitious materials, Construction and
675 Building Materials 249 (2020) 118763.
676 [40] H. Tan, K. Nie, X. He, X. Deng, X. Zhang, Y. Su, J. Yang, Compressive strength and
677 hydration of high-volume wet-grinded coal fly ash cementitious materials, Construction and
678 Building Materials 206 (2019) 248-260.
679 [41] G. Li, H. Tan, X. He, J. Zhang, X. Deng, Z. Zheng, Y. Guo, The influence of wet ground
680 fly ash on the performance of foamed concrete, Construction and Building Materials 304 (2021)
681 124676.
682 [42] X. Liu, B. Ma, H. Tan, X. He, R. Zhao, P. Chen, Y. Su, J. Yang, Preparation of ultrafine
683 fly ash by wet grinding and its utilization for immobilizing chloride ions in cement paste, Waste
684 Management 113 (2020) 456-468.
685 [43] Y. Wang, J. Li, X. He, Z. Zheng, Y. Su, H. Zhao, J. Yang, B. Strnadel, Effects of wet-
686 grinded superfine waste glass on the fresh properties and reaction characteristic of cement
687 pastes, Construction and Building Materials 247 (2020) 118593.
688 [44] S. Liu, Q. Li, G. Xie, L. Li, H. Xiao, Effect of grinding time on the particle characteristics
689 of glass powder, Powder Technology 295 (2016) 133-141.
690 [45] BS EN 1015-3, Methods of test for mortar for masonry - Part 3: Determination of
691 consistence of fresh mortar (by flow table), The British Standards Institution, UK, 1999.
692 [46] BS EN 196-3, Determination of setting times and soundness, The British Standards
693 Institution, UK, 2016.
694 [47] Y. Sun, J.-X. Lu, C.S. Poon, Strength degradation of seawater-mixed alite pastes: an
695 explanation from statistical nanoindentation perspective, Cement and Concrete Research 152
696 (2022) 106669.
697 [48] J. Menčík, D. Munz, E. Quandt, E. Weppelmann, M. Swain, Determination of elastic
698 modulus of thin layers using nanoindentation, Journal of Materials Research 12(9) (1997)
699 2475-2484.
700 [49] J. Xu, S.-Q. Shi, Investigation of mechanical properties of ε-zirconium hydride using
701 micro-and nano-indentation techniques, Journal of nuclear materials 327(2-3) (2004) 165-170.
702 [50] G. Plusquellec, M.R. Geiker, J. Lindgård, J. Duchesne, B. Fournier, K. De Weerdt,
703 Determination of the pH and the free alkali metal content in the pore solution of concrete:
704 Review and experimental comparison, Cement and Concrete Research 96 (2017) 13-26.
705 [51] J.J. Thomas, D. Rothstein, H.M. Jennings, B.J. Christensen, Effect of hydration
706 temperature on the solubility behavior of Ca-, S-, Al-, and Si-bearing solid phases in Portland
707 cement pastes, Cement and Concrete Research 33(12) (2003) 2037-2047.
708 [52] I. Klur, B. Pollet, J. Virlet, A. Nonat, CSH structure evolution with calcium content by
709 multinuclear NMR, in: P. Colombet, A.-R. Grimmer, H. Zanni, P. Sozzani (Eds.) Nuclear
710 magnetic resonance spectroscopy of cement-based materials, Springer, Berlin, 1998, pp. 119-
711 141.
712 [53] W.L. Lam, P. Shen, Y. Cai, Y. Sun, Y. Zhang, C.S. Poon, Effects of seawater on UHPC:
713 Macro and microstructure properties, Construction and Building Materials 340 (2022) 127767.
714 [54] D.K. Panesar, Supplementary cementing materials, in: S. Mindess (Ed.), Developments in
715 the Formulation and Reinforcement of Concrete, Woodhead Publishing, Duxford, UK, 2019.

[55] M. Kosmulski, M. Kalbarczyk, Zeta Potential of Nanosilica in 50% Aqueous Ethylene Glycol and in 50% Aqueous Propylene Glycol, Molecules 28(3) (2023) 1335.
[56] Q. Rusheng, Z. Yunsheng, Z. Yu, L. Cheng, Y. Lin, K. Deyu, Effects of aqueous-phase speciation on Portland cement and supplementary cementitious materials as reflected using zeta potential of powder suspensions, Construction and Building Materials 345 (2022) 128258.
[57] D.L. COCKE, H.G. McWHINNEY, D.C. DUFNER, B. HORRELL, J.D. Ortego, An XPS and EDS investigation of Portland cement doped with Pb2+ and Cr3+ cations, Hazardous waste and hazardous materials 6(3) (1989) 251-267.
[58] P. Baláž, M. Achimovičová, M. Baláž, P. Billik, Z. Cherkezova-Zheleva, J.M. Criado, F. Delogu, E. Dutková, E. Gaffet, F.J. Gotor, Hallmarks of mechanochemistry: from nanoparticles to technology, Chemical Society Reviews 42(18) (2013) 7571-7637.
[59] G.S. Islam, M. Rahman, N. Kazi, Waste glass powder as partial replacement of cement for sustainable concrete practice, International Journal of Sustainable Built Environment 6(1) (2017) 37-44.
[60] L.F. Jochem, C.A. Casagrande, L. Onghero, C. Venancio, P.J. Gleize, Effect of partial replacement of the cement by glass waste on cementitious pastes, Construction and Building Materials 273 (2021) 121704.
[61] A.M. Matos, J. Sousa-Coutinho, Durability of mortar using waste glass powder as cement replacement, Construction and building materials 36 (2012) 205-215.
[62] G. Konstantopoulos, E. Koumoulos, A. Karatza, C. Charitidis, Pore and phase identification through nanoindentation mapping and micro-computed tomography in nanoenhanced cement, Cement and Concrete Composites 114 (2020) 103741.
[63] K. Scrivener, R. Snellings, B. Lothenbach, A practical guide to microstructural analysis of cementitious materials, Taylor & Francis Group, Boca Raton, Florida, 2018.
[64] D.L. Kong, J.G. Sanjayan, Effect of elevated temperatures on geopolymer paste, mortar and concrete, Cem. Concr. Res. 40(2) (2010) 334-339.
[65] Z. Wu, K.H. Khayat, C. Shi, B.F. Tutikian, Q. Chen, Mechanisms underlying the strength enhancement of UHPC modified with nano-SiO2 and nano-CaCO3, Cem. Concr. Compos. 119 (2021) 103992.
[66] L. Wang, H. Yang, S. Zhou, E. Chen, S. Tang, Hydration, mechanical property and CSH structure of early-strength low-heat cement-based materials, Materials Letters 217 (2018) 151-154.
[67] C. Pichler, R. Lackner, Post-peak decelerating reaction of Portland cement: Monitoring by heat flow calorimetry, modelling by Elovich-Landsberg model and reaction-order model, Construction and Building Materials 231 (2020) 117107.
[68] I. Jawed, J. Skalny, Alkalies in cement: a review: II. Effects of alkalies on hydration and performance of Portland cement, Cement and concrete research 8(1) (1978) 37-51.
[69] H.F.W. Taylor, Cement Chemistry, 2 ed., Thomas Telford Publishing, New York, NY, 1997.
[70] K. Zheng, Pozzolanic reaction of glass powder and its role in controlling alkali–silica reaction, Cement and Concrete Composites 67 (2016) 30-38.
[71] X. Gao, Q. Yu, X. Li, Y. Yuan, Assessing the modification efficiency of waste glass powder in hydraulic construction materials, Construction and Building Materials 263 (2020) 120111.
[72] J. Cheung, A. Jeknavorian, L. Roberts, D. Silva, Impact of admixtures on the hydration kinetics of Portland cement, Cement and concrete research 41(12) (2011) 1289-1309.
[73] F. Lin, C. Meyer, Hydration kinetics modeling of Portland cement considering the effects of curing temperature and applied pressure, Cement and Concrete Research 39(4) (2009) 255-265.

765 [74] H. Zheng, J.-G. Dai, C.S. Poon, W. Li, Influence of calcium ion in concrete pore solution
766 on the passivation of galvanized steel bars, Cement and Concrete Research 108 (2018) 46-58.
767 [75] A.A. de Moura, L. Effting, M.P. Moisés, G.G.A. Carbajal, C.R.T. Tarley, E. Câmara, A.
768 Gracioli, A. Bail, The influence of calcium-rich environments in siliceous industrial residues
769 on the hydration reaction of cementitious mixtures, Journal of Cleaner Production 225 (2019)
770 152-162.
771 [76] J. Wu, Q. Ding, W. Yang, L. Wang, H. Wang, Influence of Submicron Fibrillated
772 Cellulose Fibers from Cotton on Hydration and Microstructure of Portland Cement Paste,
773 Molecules 26(19) (2021) 5831.
774